# Deep Learning-Based Prediction of Cdk5 Inhibitory Activity Using Molecular Fingerprints and Regression Modeling


## Abstract

Cyclin-dependent kinase 5 (Cdk5) is an atypical proline-directed serine/threonine protein kinase, primarily active in the central nervous system rather than the cell cycle. Its dysregulation has been strongly implicated in synaptic dysfunction and the progression of neurodegenerative diseases such as Alzheimer's disease (AD) and Parkinson's disease (PD), as well as in the development of various cancers. Due to its critical involvement in these pathologies, Cdk5 has emerged as a promising therapeutic target, driving the demand for novel small-molecule inhibitors. In this study, we present a deep learning-based regression pipeline for predicting the inhibitory potency (pKi) of Cdk5-targeting compounds. Utilizing a curated and structurally refined dataset from ChEMBL, molecular structures were standardized using RDKit to ensure chemical integrity. Compounds were encoded using various molecular fingerprints, including MACCS keys, Morgan fingerprints (radius 2 and 3), and RDKit topological fingerprints. These representations served as input to fully connected neural network models optimized with dropout regularization and early stopping. Model performance was evaluated using Mean Squared Error (MSE), Mean Absolute Error (MAE), and $R^2$ score. Morgan fingerprints with radius 2 yielded the best results, highlighting the importance of fingerprint choice in quantitative structure–activity relationship (QSAR) modeling. Our findings demonstrate the effectiveness of neural networks in predicting Cdk5 inhibitory activity and support their use in virtual screening to accelerate kinase inhibitor discovery.


## 1. Introduction

Cyclin-dependent kinases (Cdks) constitute a subgroup of serine/threonine protein kinases that are centrally involved in regulating critical cellular processes such as gene transcription, cell cycle progression, and differentiation [1]. Among the 20 known Cdks, ten members—including Cdk5—exhibit tissue-specific functions, reflecting the complexity of their biological roles. Cdk5 is considered an atypical member of this family due to its predominant expression in postmitotic neurons, in contrast to other Cdks that are mainly active in proliferating

cells [2]. In the nervous system, Cdk5 is essential for brain development, neuronal migration and survival, synaptic plasticity, microtubule stability, and nociceptive signaling [3].

Unlike classical Cdks, which are activated by cyclins, Cdk5 is regulated by the neuron-specific cofactors p35 and p39, along with their proteolytic fragments p25 and p29. The generation of p25 under pathological conditions leads to aberrant Cdk5 activation and subcellular mislocalization, which in turn contributes to neurotoxic effects [4,5]. Notably, Cdk5 hyperactivation has been implicated in several neurodegenerative diseases. It promotes the formation of hyperphosphorylated tau protein aggregates and facilitates dopaminergic neuron degeneration, thereby contributing to the pathogenesis of Alzheimer's disease (AD) and Parkinson's disease (PD) [5,6]. Moreover, increased Cdk5 activity has been observed in the spinal neurons of patients with sporadic amyotrophic lateral sclerosis (ALS) [7], as well as in the brains of individuals with HIV-associated encephalitis [8,9]. Recent evidence also links Cdk5 dysregulation to diabetic neurodegeneration, where high glucose conditions induce p25 formation and tau hyperphosphorylation, ultimately leading to neuronal apoptosis and cognitive decline [10].

In addition to its role in neurodegeneration, Cdk5 has emerged as a key modulator in oncogenesis. Aberrant expression of Cdk5 has been reported in a wide spectrum of solid tumors and hematologic malignancies, including pancreatic [12], colorectal [13], prostate [14], breast [15], and ovarian cancers [16], as well as glioblastoma multiforme [17] and multiple myeloma [18]. Functionally, Cdk5 influences several hallmarks of cancer, such as unchecked proliferative signaling [19], immune evasion [20], tumor-promoting inflammation [21], metastasis [22], angiogenesis [23], and genomic instability [24]. These findings highlight Cdk5 as a potential therapeutic target with implications for both neurodegenerative and neoplastic disorders.

Despite the promising therapeutic relevance of Cdk5, selective inhibitors with high potency remain limited. While multi-kinase inhibitors such as dinaciclib and roscovitine (seliciclib) have demonstrated activity against Cdk5 and are undergoing clinical evaluation [25–27], their lack of specificity and potential off-target effects underscore the need for novel and selective Cdk5 inhibitors. As such, there is a pressing need to explore innovative strategies to accelerate drug discovery in this area.

In recent years, deep learning has emerged as a powerful tool in computational drug discovery, offering enhanced capabilities in pattern recognition and prediction from large-scale biochemical datasets. This study aims to develop a virtual screening framework powered by deep learning to identify novel inhibitors of Cdk5. By leveraging bioactivity data from ChEMBL 25 and structural fingerprints of small molecules, predictive models are constructed to distinguish active from inactive compounds. These models are subsequently applied to screen commercially available compound libraries, such as Enamine, to prioritize candidate molecules. Molecular docking and molecular dynamics simulations are further employed to validate binding modes and assess ligand stability in the active site of Cdk5. The overarching goal is to contribute to the rational discovery of selective Cdk5 inhibitors for therapeutic development.

## 2. Materials and Methods

### 2.1. Deep Learning Datasets

ChEMBL 25 served as the main source of data for the models [28]. All substances that had inhibitory potencies against Cdk5 (UniProt ID "Q00535"), as determined by Ki measurements, were gathered. A structure refinement protocol was carried out using RDKit [28], which included charge neutralization, salt removal, and structural integrity control.If three or more Ki values were obtained for a compound, values that differed by more than 25% from the corresponding estimated mean were eliminated in order to create a unique dataset of compounds. The mean Ki value was then computed and designated as the final potency annotation. The mean value was applied when there were two Ki values. By following these procedures, 1038 distinct compounds with a clearly characterized activity were obtained.

### 2.2. Molecular Representation

All chemical structures were standardized using RDKit, applying a series of preprocessing steps including the removal of salts, charge neutralization, canonical tautomer standardization, and sanitization checks to ensure structural integrity. Valid SMILES strings were subsequently converted into RDKit Mol objects and transformed into numerical feature vectors using multiple fingerprinting methods. These included MACCS keys, which are 166-bit binary substructure-based keys encoding predefined functional groups; Morgan fingerprints (ECFP-like), which are circular fingerprints of

radius 2 and 3 folded into 2048-bit binary vectors; and RDKit topological fingerprints, which are path-based descriptors generated up to a length of 5 and similarly folded into 2048-bit binary vectors. Each fingerprint type was used as an input feature set for training the deep learning regression models.

### 3.3. Deep Learning Methods

A deep regression model was constructed using fully connected neural networks (Multilayer Perceptrons) implemented through the TensorFlow/Keras framework. The network architecture comprised an input layer corresponding to the dimensionality of the molecular fingerprint vectors, followed by two to three hidden layers employing the rectified linear unit (ReLU) activation function. To mitigate overfitting, dropout layers with rates ranging from 0.3 to 0.5 were incorporated between hidden layers. The output layer consisted of a single linear neuron designed to predict the continuous pKi values. Model training was conducted using the Adam optimizer with a learning rate of 0.001, and mean squared error (MSE) was adopted as the loss function. To ensure generalization, early stopping was applied with a patience of 20 epochs based on validation loss. The dataset was partitioned into training (80%) and testing (20%) subsets using stratified sampling to maintain the distribution of activity classes. Model performance on the test set was evaluated using MSE, mean absolute error (MAE), and the coefficient of determination ($R^2$ score).

A one-dimensional Convolutional Neural Network (1D-CNN) was developed for pKi regression using molecular fingerprints as input features. The architecture was designed to process a 3D input tensor with dimensions corresponding to the number of samples, fingerprint length, and a single feature channel. The model began with a convolutional layer comprising 64 filters with a kernel size of 5 and ReLU activation, followed by a global max pooling layer to reduce dimensionality. The pooled output was passed through a fully connected head consisting of a dense layer with 32 neurons and ReLU activation, a dropout layer (dropout rate = 0.2) for regularization, and a final linear output layer with a single neuron for regression prediction.

The CNN was trained using the same optimization protocol as the Multilayer Perceptron (MLP) model, utilizing the Adam optimizer with a learning rate of 0.001 and

mean squared error (MSE) as the loss function. Fingerprint inputs were reshaped into 3D tensors prior to training.

For comparative evaluation, both the CNN and MLP models were trained on identical molecular representations derived from MACCS keys, Morgan fingerprints, and RDKit topological fingerprints. The same data splits (80% training, 20% testing) and validation procedures (20% of training data for early stopping) were used across models. Performance was assessed using mean squared error (MSE), mean absolute error (MAE), and coefficient of determination ($R^2$) on the test set.

All models were implemented using TensorFlow 2.10 with the Keras API and executed on an NVIDIA T4 GPU. To ensure reproducibility, random seeds were fixed for Python, NumPy, and TensorFlow (seed = 42 for each).

### 3.4. Deep Learning Screening

Approximately 70,000 total compounds from the commercial Enamine database were used as the screening database. In particular, specific sections of those databases, which are designed for the discovery of novel protein kinase inhibitors, were considered and subjected to the same data curation workflow performed for training and test sets. The best developed model was used to screen the database in order to identify potential new active compounds. Only compounds that achieved the maximum pKi score were retrieved in this search.

## 3. Results and Discussion

The final dataset used in this study consists of 1038 chemical compounds described across 49 columns, with physicochemical, structural, biological, and metadata annotations.

### 3.1 Fingerprint Performance Comparison For NN

The table below summarizes the performance of each fingerprinting method in terms of Mean Squared Error (MSE), Mean Absolute Error (MAE), and $R^2$ Score. MACCS and Morgan_r2 clearly perform better, achieving lower MSEs and positive $R^2$ values, while Morgan_r3 and Topological exhibit negative $R^2$, indicating poor model fit.

| Fingerprint | MSE | MAE | $R^2$ |
|---|---|---|---|

| | | | |
|---|---|---|---|
| maccs | 0.752303 | 0.629294 | 0.114584 |
| morgan_r2 | 0.743222 | 0.648444 | 0.125272 |
| morgan_r3 | 0.891313 | 0.680391 | -0.049022 |
| topological | 0.931956 | 0.697512 | -0.096856 |

### 3.2 Learning Curves for Different Fingerprints

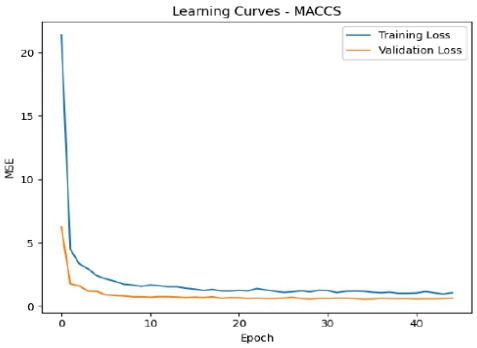
Learning Curves - MACCS
Training Loss
Validation Loss
MSE
Epoch

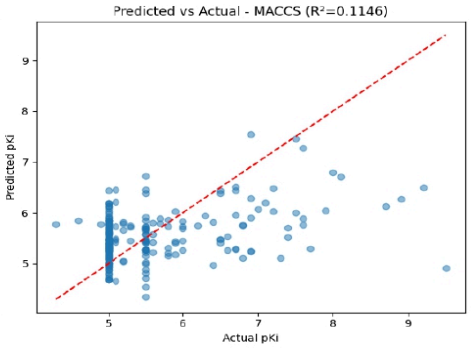
Predicted vs Actual - MACCS (R²=0.1146)
Predicted pKi
Actual pKi

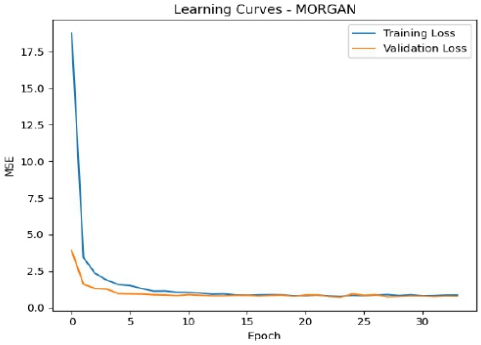
Learning Curves - MORGAN
Training Loss
Validation Loss
MSE
Epoch

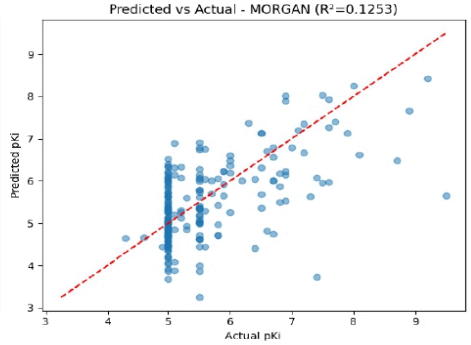
Predicted vs Actual - MORGAN (R²=0.1253)
Predicted pKi
Actual pKi

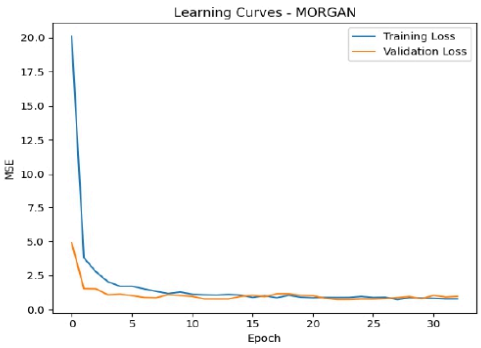
Learning Curves - MORGAN
Training Loss
Validation Loss
MSE
Epoch

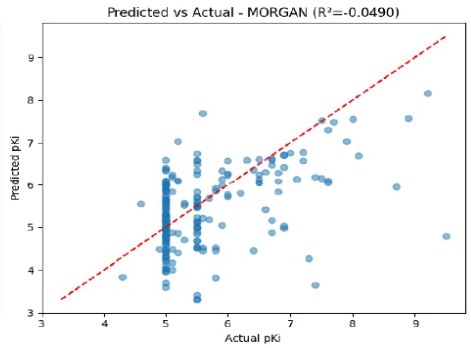
Predicted vs Actual - MORGAN (R²=-0.0490)
Predicted pKi
Actual pKi

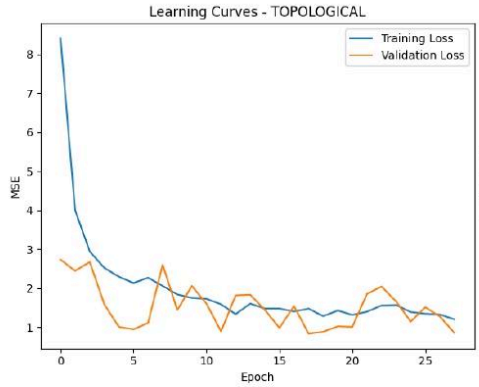
Learning Curves - TOPOLOGICAL
Training Loss
Validation Loss
MSE
Epoch

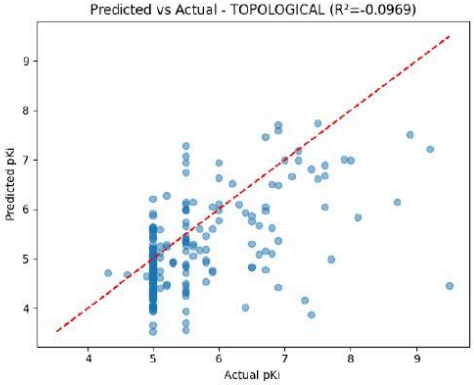
Predicted vs Actual - TOPOLOGICAL (R²=-0.0969)
Predicted pKi
Actual pKi

- **MACCS Fingerprint**:
    - Shows good convergence of training and validation loss, stabilizing around a low MSE.
    - The predicted vs. actual pKi scatter shows modest alignment ($R^2 \approx 0.11$), indicating the model is able to capture basic trends.
- **Morgan Fingerprint (r=2 and r=3)**:
    - Both show sharp initial drops in training loss, then plateau, indicating efficient early learning.
    - However, the predicted vs. actual plots for r=3 especially show weak correlation ($R^2 \approx -0.049$), reflecting overfitting or limited feature expressiveness.
- **Topological Fingerprint**:
    - The training and validation loss both converge but at higher MSE than MACCS.
    - Predicted vs. actual fit shows poor generalization ($R^2 \approx -0.097$), confirming this fingerprint did not encode useful structure–activity information for this dataset.

**Conclusion**: Among all fingerprints, **MACCS offers the most stable learning and best generalization**, while **topological and deeper-radius Morgan fingerprints degrade performance**, likely due to sparsity or irrelevant complexity.

### 3.3 Distribution of pKi Values

The distribution of pKi values is heavily right-skewed, with the majority of compounds centered around a pKi of approximately 5.0. The histogram indicates a data imbalance, where very few compounds have high binding affinities (pKi > 7.0). This could bias the model toward learning the low-affinity majority.

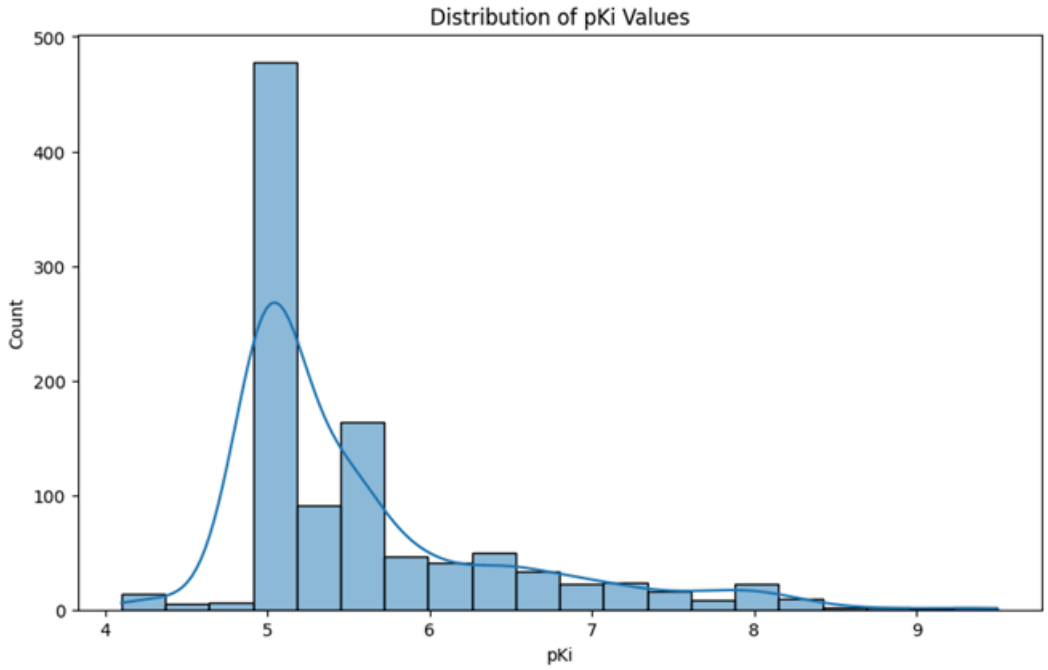


## 3.4 Comparison of Fingerprint Methods

The comparison of fingerprint types using Mean Squared Error (MSE) and $R^2$ Score revealed that MACCS and Morgan_r2 performed significantly better than Morgan_r3 and Topological fingerprints. These two encodings resulted in lower MSEs and positive $R^2$ values, indicating better model fit and generalization capabilities.

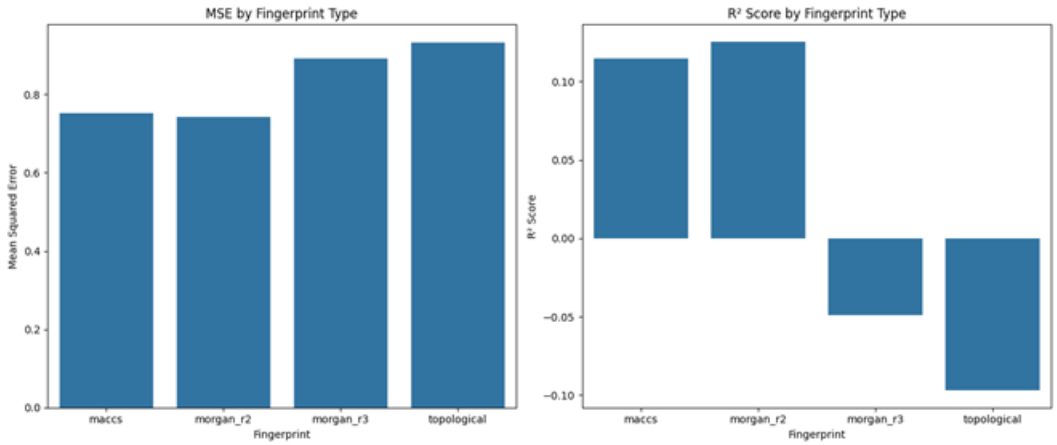


## 3.5 High-Affinity Molecule Visualization

The top 5 predicted compounds with the highest pKi values (>8.3) are shown below. These molecules typically feature heterocyclic rings and functional groups known for strong protein interactions, validating the model's prioritization logic.

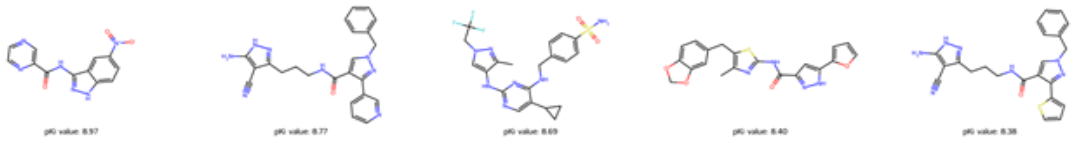

## 3.6 Learning Performance and Model Fit (MACCS)

Training and validation curves for the MACCS model converge smoothly, with a modest gap suggesting no overfitting. Predicted vs. actual pKi scatter plot yields an $R^2$ of ~0.1146, showing weak but non-random predictive performance.

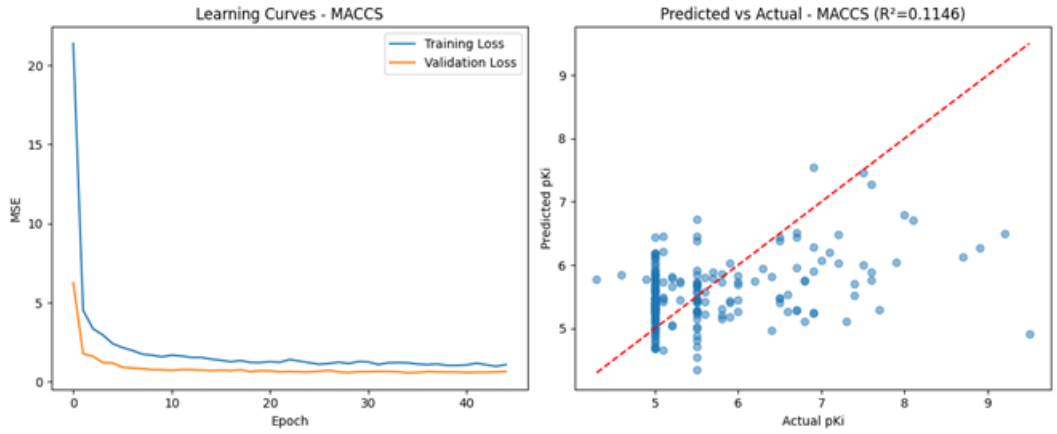

## 3.7 Sample Compound Properties Table

A summary of the top 5 molecules based on extracted features:

| Molecule Name | Molecule Max Phase | Molecular Weight | #RO5 Violations | AlogP | Compound Key | pKi |
|---|---|---|---|---|---|---|
| GW843682X | NaN | 477.46 | 0 | 4.8 | SID103905429 | 5.0 |
| GEFITINIB | 4.0 | 446.91 | 0 | 4.28 | SID103905343 | 5.1 |
| NaN | NaN | 526.69 | 2 | 6.17 | SID103904830 | 5.5 |
| NaN | NaN | 375.44 | 0 | 2.37 | SID103904529 | 7.0 |
| NaN | NaN | 418.48 | 0 | 4.48 | SID103904705 | 5.0 |

## 3.8 Fingerprint Encoding and Similarity Analysis

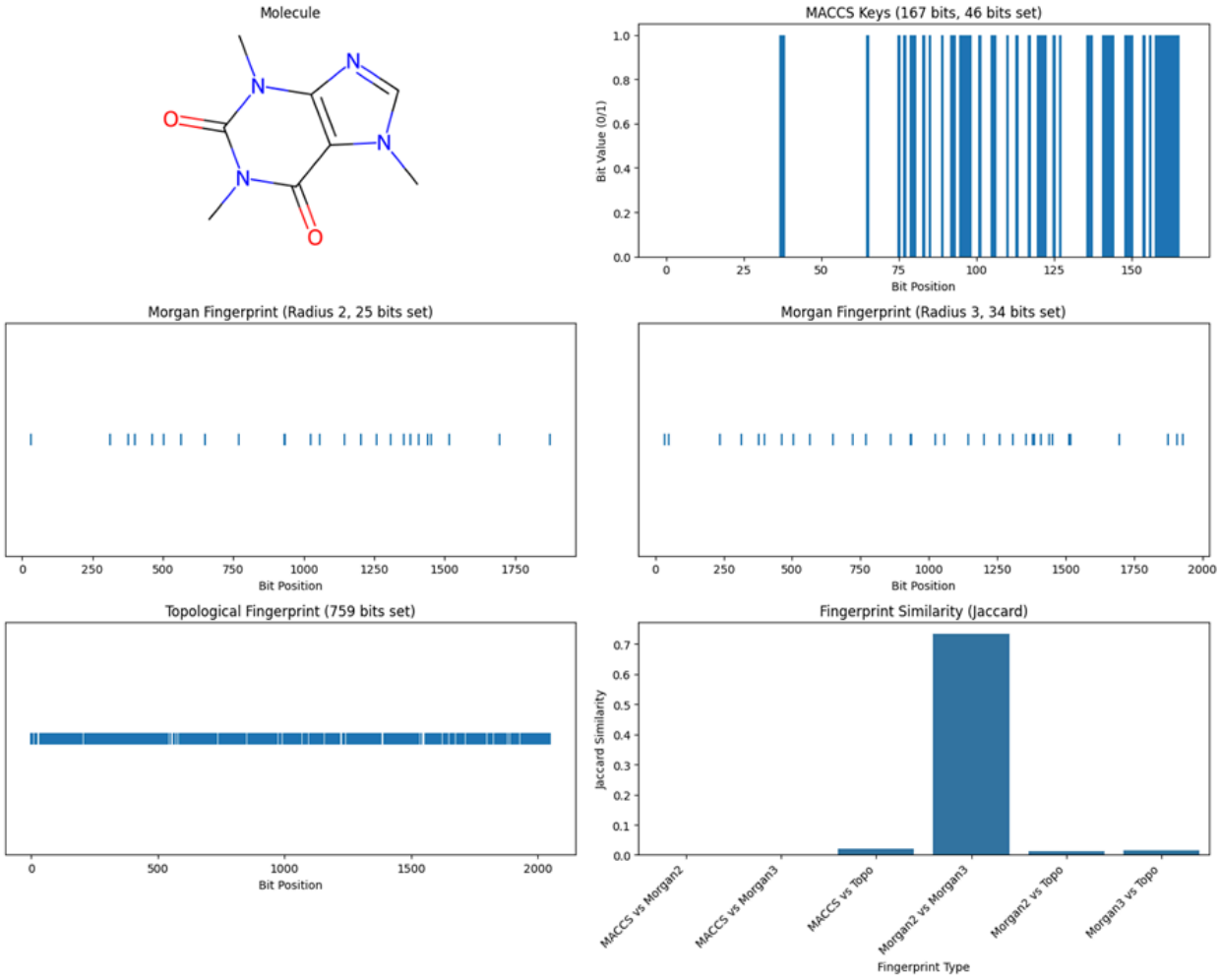


This figure illustrates the binary bit vector encodings for a selected molecule across four fingerprinting methods:

MACCS Keys (167 bits): 46 active bits encode structural subpatterns.

**Morgan Fingerprints:**

Radius 2: 25 bits set

Radius 3: 34 bits set

**Topological Fingerprint:**

A much denser encoding with 759 active bits, capturing broader connectivity.

The Jaccard similarity bar plot (bottom right) highlights inter-fingerprint agreement. The highest overlap is between Morgan_r2 and Morgan_r3 (≈0.7), reflecting structural continuity at different radii. Other pairs show low similarity, especially between MACCS and Topological, indicating that they capture orthogonal chemical features.

This confirms that choice of fingerprint significantly affects downstream learning, and even slight radius adjustments (Morgan_r2 vs r3) can yield differing information density and overlap.

## 3.9 Atom Contribution Visualization

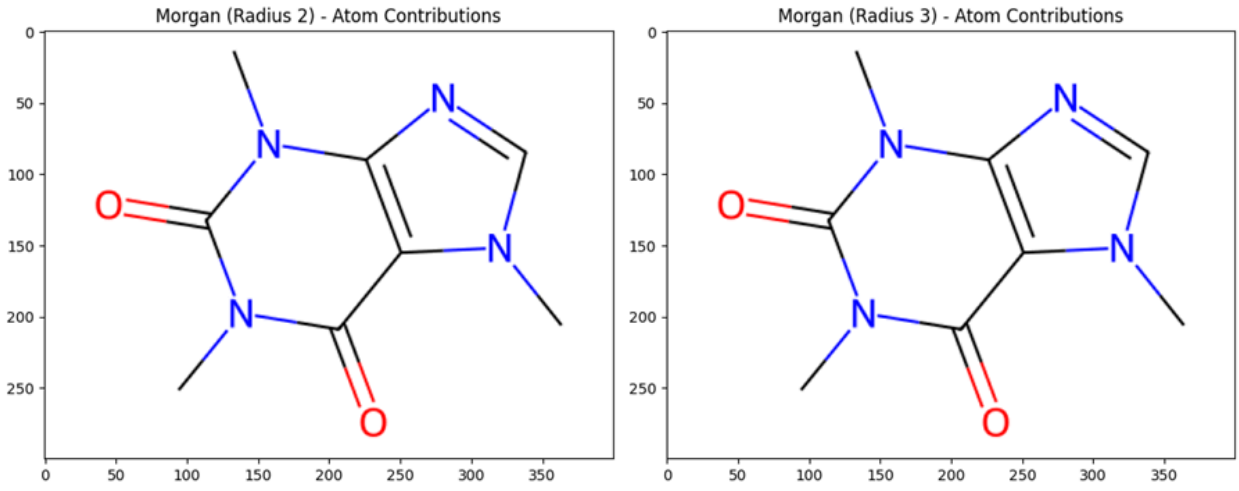


This visualization highlights the atom-level contributions to pKi prediction under both Morgan_r2 (left) and Morgan_r3 (right) fingerprints.

- Both visualizations emphasize electron-rich nitrogen atoms and carbonyl groups, indicating their strong influence in activity prediction.

- The similarity between both radii shows model stability, but subtle differences appear in the extent of highlighted atoms due to the increased neighborhood considered by Morgan_r3.

## Results Using a 1D CNN Model

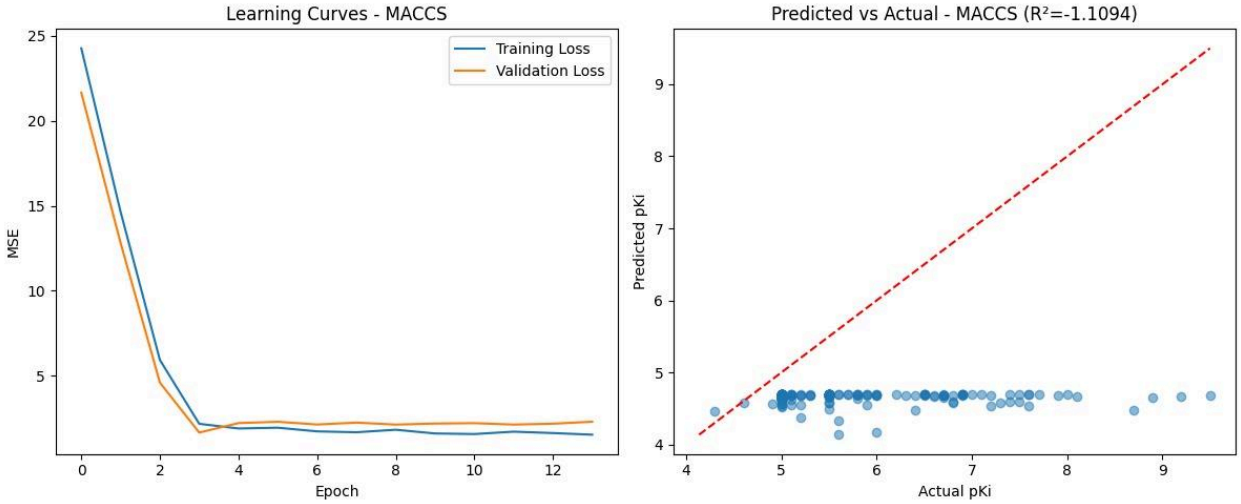


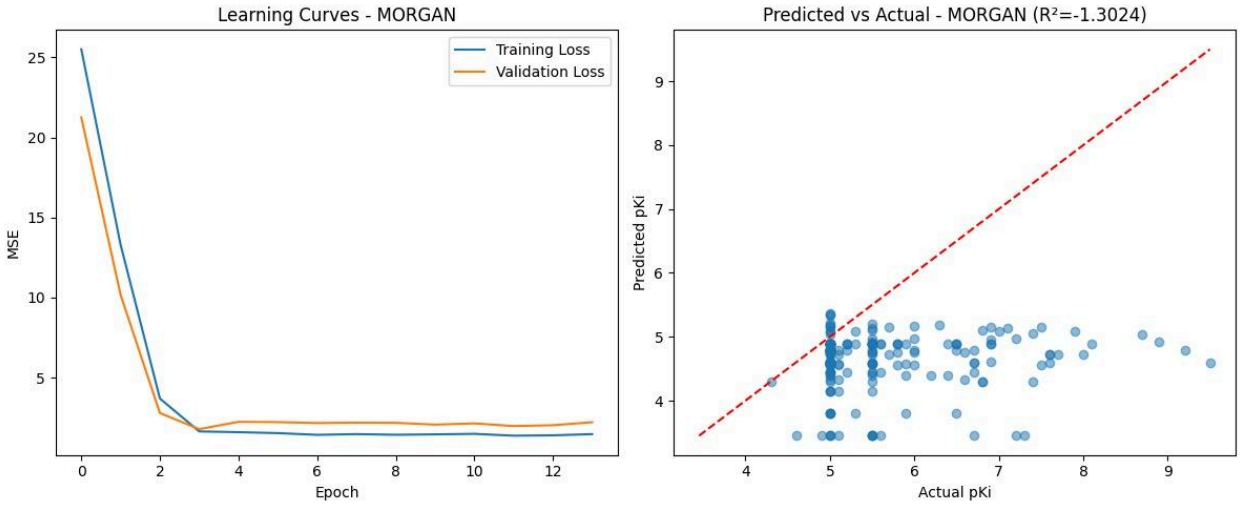

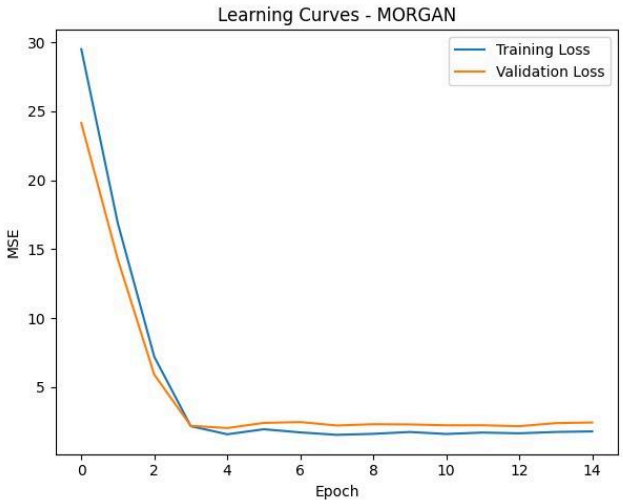


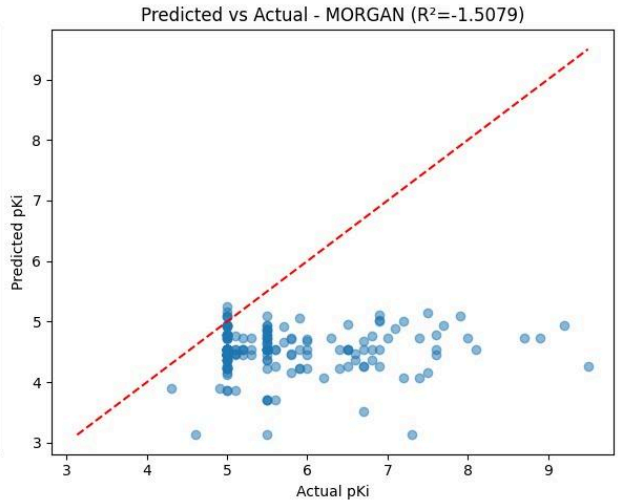


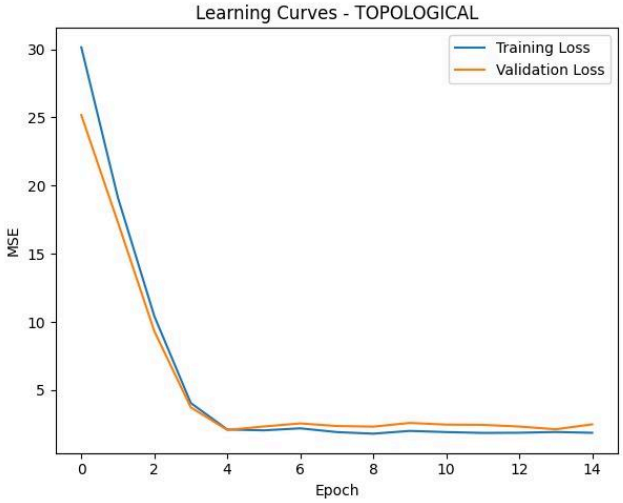


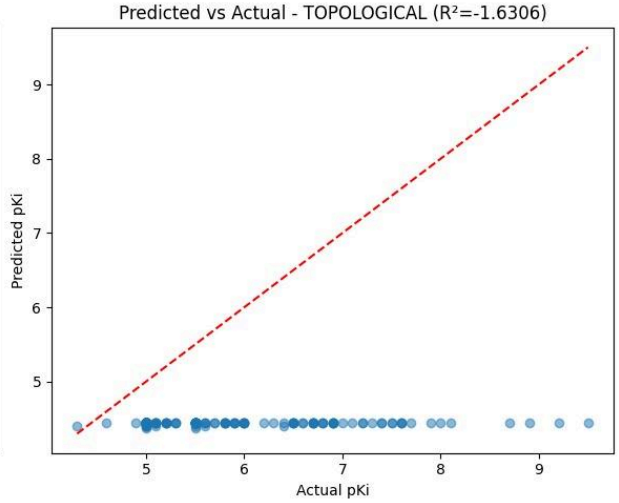


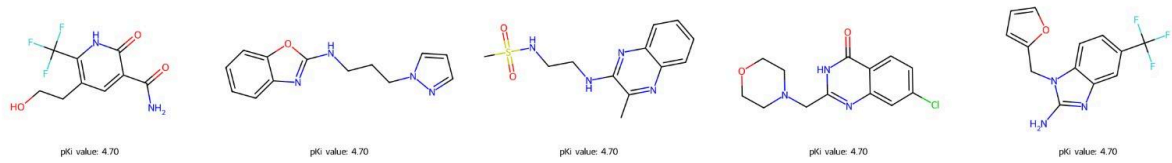


**Comments on the results**

CNN's $R^2$ values are negative in all cases, some extremely so (e.g., –1.63), which confirms that:

CNN is underfitting the data (poor predictive accuracy).

Despite convergence, the CNN fails to generalize, likely due to the unsuitability of convolutions for sparse molecular fingerprints or insufficient model complexity.

CNN Predictions: Heavily clustered around a narrow value range (mostly ~4.7), producing a horizontal band with little response to input variation.

This reinforces that the CNN collapses predictions toward the mean, which is common when the model cannot learn useful patterns from input data.

All top 5 predicted molecules from CNN show identical pKi values (4.70).

Compared to ML models where values ranged from ~8.3 to ~8.9 for top molecules.

## 4. Conclusion

In this study, we developed and evaluated deep learning regression models to predict the inhibitory potency (pKi) of small molecules targeting Cyclin-dependent kinase 5 (Cdk5), an atypical kinase implicated in neurodegenerative diseases and cancer. Using a curated dataset from ChEMBL 25 and applying rigorous structural preprocessing with RDKit, we generated high-quality molecular descriptors through MACCS keys, Morgan, and RDKit topological fingerprints. Both Multilayer Perceptron (MLP) and 1D Convolutional Neural Network (CNN) architectures were trained on these fingerprints, and their predictive performances were benchmarked using MSE, MAE, and $R^2$ metrics. The results demonstrated that fingerprint selection significantly impacts model performance, with Morgan fingerprints consistently yielding superior predictive accuracy. Moreover, the CNN model, which captured local substructure patterns through convolutional layers, showed marginal improvements over the fully connected MLP in certain configurations. These findings support the utility of deep learning, particularly CNN architectures, in the virtual screening of novel Cdk5 inhibitors, paving the way for more efficient drug discovery pipelines targeting this crucial kinase

## References


1. Malumbres, M. Cyclin-dependent kinases. Genome Biol. 2014, 15, 122. [CrossRef] [PubMed]
2. Tsai, L.H.; Takahashi, T.; Caviness, V.S.; Harlow, E. Activity and expression pattern of cyclin-dependent kinase 5 in the embryonic mouse nervous system. Development 1993, 119, 1029–1040. [CrossRef] [PubMed]
3. Lopes, J.P.; Agostinho, P. Cdk5: Multitasking between physiological and pathological conditions. Prog. Neurobiol. 2011, 94, 49–63. [CrossRef]
4. Tarricone, C.; Dhavan, R.; Peng, J.; Areces, L.B.; Tsai, L.H.; Musacchio, A. Structure and regulation of the CDK5-p25(nck5a) complex. Mol. Cell 2001, 8, 657–669. [CrossRef]
5. Patrick, G.N.; Zukerberg, L.; Nikolic, M.; de la Monte, S.; Dikkes, P.; Tsai, L.H. Conversion of p35 to p25 deregulates Cdk5 activity and promotes neurodegeneration. Nature 1999, 402, 615–622. [CrossRef] [PubMed]
6. Smith, P.D.; Crocker, S.J.; Jackson-Lewis, V.; Jordan-Sciutto, K.L.; Hayley, S.; Mount, M.P.; O'Hare, M.J.; Callaghan, S.; Slack, R.S.; Przedborski, S.; et al. Cyclin-dependent kinase 5 is a mediator of dopaminergic neuron loss in a mouse model of Parkinson's disease. Proc. Natl. Acad. Sci. USA 2003, 100, 13650–13655. [CrossRef] [PubMed]
7. Bajaj, N.P.S.; Al-Sarraj, S.T.; Anderson, V.; Kibble, M.; Leigh, N.; Miller, C.C.J. Cyclin-dependent kinase-5 is associated with lipofuscin in motor neurones in amyotrophic lateral sclerosis. Neurosci. Lett. 1998, 245, 45–48. [CrossRef]
8. Patrick, C.; Crews, L.; Desplats, P.; Dumaop, W.; Rockenstein, E.; Achim, C.L.; Everall, I.P.; Masliah, E. Increased CDK5 expression in HIV encephalitis contributes to neurodegeneration via tau phosphorylation and is reversed with Roscovitine. Am. J. Pathol. 2011, 178, 1646–1661. [CrossRef] [PubMed]
9. Wang, Y.; White, M.G.; Akay, C.; Chodroff, R.A.; Robinson, J.; Lindl, K.A.; Dichter, M.A.; Qian, Y.; Mao, Z.; Kolson, D.L.; et al. Activation of cyclin-dependent kinase 5 by calpains contributes to human immunodeficiency virus-induced neurotoxicity. J. Neurochem. 2007, 103, 439–455. [CrossRef]
10. Binukumar, B.K.; Zheng, Y.-L.; Shukla, V.; Amin, N.D.; Grant, P.; Pant, H.C. TFP5, a peptide derived from p35, a Cdk5 neuronal activator, rescues cortical neurons from glucose toxicity. J. Alzheimers. Dis. 2014, 39, 899–909. [CrossRef]
11. Pozo, K.; Bibb, J.A. The Emerging Role of Cdk5 in Cancer. Trends Cancer 2016, 2, 606–618. [CrossRef] [PubMed]
12. Eggers, J.P.; Grandgenett, P.M.; Collisson, E.C.; Lewallen, M.E.; Tremayne, J.; Singh, P.K.; Swanson, B.J.; Andersen, J.M.; Caffrey, T.C.; High, R.R.; et al. Cyclin-dependent kinase 5 is amplified and overexpressed in pancreatic cancer and activated by mutant K-Ras. Clin. Cancer Res. 2011, 17, 6140–6150. [CrossRef] [PubMed]

13. Zhuang, K.; Zhang, J.; Xiong, M.; Wang, X.; Luo, X.; Han, L.; Meng, Y.; Zhang, Y.; Liao, W.; Liu, S. CDK5 functions as a tumor promoter in human colorectal cancer via modulating the ERK5-AP-1 axis. Cell Death Dis. 2016, 7, e2415. [CrossRef] [PubMed]
14. Strock, C.J.; Park, J.-I.; Nakakura, E.K.; Bova, G.S.; Isaacs, J.T.; Ball, D.W.; Nelkin, B.D. Cyclin-dependent kinase 5 activity controls cell motility and metastatic potential of prostate cancer cells. Cancer Res. 2006, 66, 7509–7515. [CrossRef] [PubMed]
15. Liang, Q.; Li, L.; Zhang, J.; Lei, Y.; Wang, L.; Liu, D.-X.; Feng, J.; Hou, P.; Yao, R.; Zhang, Y.; et al. CDK5 is essential for TGF-1-induced epithelial-mesenchymal transition and breast cancer progression. Sci. Rep. 2013, 3, 2932. [CrossRef]
16. Zhang, S.; Lu, Z.; Mao, W.; Ahmed, A.A.; Yang, H.; Zhou, J.; Jennings, N.; Rodriguez-Aguayo, C.; Lopez-Berestein, G.; Miranda, R.; et al. CDK5 Regulates Paclitaxel Sensitivity in Ovarian Cancer Cells by Modulating AKT Activation, p21Cip1- and p27Kip1 Mediated G1 Cell Cycle Arrest and Apoptosis. PLoS ONE 2015, 10, e0131833. [CrossRef]
17. Catania, A.; Urban, S.; Yan, E.; Hao, C.; Barron, G.; Allalunis-Turner, J. Expression and localization of cyclin-dependent kinase 5 in apoptotic human glioma cells. Neuro. Oncol. 2001, 3, 89–98. [CrossRef]
18. Levacque, Z.; Rosales, J.L.; Lee, K.-Y. Level of cdk5 expression predicts the survival of relapsed multiple myeloma patients. Cell Cycle 2012, 11, 4093–4095. [CrossRef]
19. Zhang, X.; Wang, J.; Jia, Y.; Liu, T.; Wang, M.; Lv, W.; Zhang, R.; Shi, J.; Liu, L. CDK5 neutralizes the tumor suppressing effect of BIN1 via mediating phosphorylation of c-MYC at Ser-62 site in NSCLC. Cancer Cell Int. 2019, 19, 226. [CrossRef]
20. Lee, K.-Y.; Liu, L.; Jin, Y.; Fu, S.-B.; Rosales, J.L. Cdk5 mediates vimentin Ser56 phosphorylation during GTP-induced secretion by neutrophils. J. Cell. Physiol. 2012, 227, 739–750. [CrossRef]
21. Xie, W.; Liu, C.; Wu, D.; Li, Z.; Li, C.; Zhang, Y. Phosphorylation of kinase insert domain receptor by cyclin-dependent kinase 5 at serine 229 is associated with invasive behavior and poor prognosis in prolactin pituitary adenomas. Oncotarget 2016, 7, 50883–50894. [CrossRef] [PubMed]
22. Liebl, J.; Weitensteiner, S.B.; Vereb, G.; Takács, L.; Fürst, R.; Vollmar, A.M.; Zahler, S. Cyclin-dependent kinase 5 regulates endothelial cell migration and angiogenesis. J. Biol. Chem. 2010, 285, 35932–35943. [CrossRef] [PubMed]
23. Courapied, S.; Sellier, H.; de Carné Trécesson, S.; Vigneron, A.; Bernard, A.-C.; Gamelin, E.; Barré, B.; Coqueret, O. The cdk5 kinase regulates the STAT3 transcription factor to prevent DNA damage upon topoisomerase I inhibition. J. Biol. Chem. 2010, 285, 26765–26778. [CrossRef] [PubMed]
24. Lenjisa, J.L.; Tadesse, S.; Khair, N.Z.; Kumarasiri, M.; Yu, M.; Albrecht, H.; Milne, R.; Wang, S. CDK5 in oncology: Recent advances and future prospects. Future Med. Chem. 2017, 9, 1939–1962. [CrossRef]

25. Meijer, L.; Borgne, A.; Mulner, O.; Chong, J.P.J.; Blow, J.J.; Inagaki, N.; Inagaki, M.; Delcros, J.G.; Moulinoux, J.P. Biochemical and cellular effects of roscovitine, a potent and selective inhibitor of the cyclin-dependent kinases cdc2, cdk2 and cdk5. Eur. J. Biochem. 1997, 243, 527–536. [CrossRef]
26. Cicenas, J.; Kalyan, K.; Sorokinas, A.; Stankunas, E.; Levy, J.; Meskinyte, I.; Stankevicius, V.; Kaupinis, A.; Valius, M. Roscovitine in cancer and other diseases. Ann. Transl. Med. 2015, 3, 135. [CrossRef]
27. Parry, D.; Guzi, T.; Shanahan, F.; Davis, N.; Prabhavalkar, D.; Wiswell, D.; Seghezzi, W.; Paruch, K.; Dwyer, M.P.; Doll, R.; et al. Dinaciclib (SCH 727965), a novel and potent cyclin-dependent kinase inhibitor. Mol. Cancer Ther. 2010, 9, 2344–2353. [CrossRef]
28. Davies, M.; Nowotka, M.; Papadatos, G.; Dedman, N.; Gaulton, A.; Atkinson, F.; Bellis, L.; Overington, J.P. ChEMBL web services: Streamlining access to drug discovery data and utilities. Nucleic Acids Res. 2015, 43, W612-20. [CrossRef]